

# MORPHOLOGIES IN A CLUSTER OF EXTREMELY RED GALAXIES WITH OLD STELLAR POPULATIONS AT $Z = 1.34$ <sup>1</sup>

HAI FU, ALAN STOCKTON, AND MICHAEL LIU<sup>2</sup>

Institute for Astronomy, University of Hawaii, 2680 Woodlawn Drive, Honolulu, HI 96822

*accepted for publication in ApJ*

## ABSTRACT

We have identified a clustering of red galaxies from deep optical/IR images obtained as part of the Institute for Astronomy Deep Survey. Photometric spectral-energy distributions indicate that most of these galaxies comprise nearly pure old stellar populations at a redshift near 1.4, and Keck spectroscopy of the three brightest red galaxies confirm this interpretation and give redshifts ranging from 1.335 to 1.338. Four of the galaxies are close together on the sky and less than  $30''$  from an  $R = 13.5$  star, and we have obtained deep adaptive-optics imaging of this group. Detailed analysis and modeling of the surface-brightness profiles of these galaxies shows that two are normal ellipticals, one is an S0, and one appears to be an essentially pure disk of old stars, with no significant bulge. All four are highly relaxed, symmetric systems. While the old, bulgeless disk galaxy represents a type that is rare at the present epoch, the other three galaxies have structural parameters that are essentially indistinguishable from those of present-day galaxies and differ only in the age of their stellar populations.

*Subject headings:* galaxies: high-redshift—galaxies: formation—galaxies: evolution

## 1. INTRODUCTION

Clusters of galaxies at high redshifts are important both because their number density as functions of mass and redshift can constrain cosmological models and because they provide samples of galaxies in dense environments for studies of galaxy formation and evolution. X-ray surveys published to date, spectacularly successful at locating massive clusters out to  $z \sim 0.7$  (e.g., Ebeling, Edge, & Henry 2001; Mullis et al. 2003), have not had the sensitivity to produce significant samples at  $z > 1$ . Surveys currently under way with XMM-Newton show promise of extending the range for well characterized samples to  $z \sim 1.5$  (e.g., Schwobe et al. 2004; Mullis et al. 2005). In the meantime, optical/IR approaches to cluster detection are undergoing a renaissance through the use of photometric redshift information in multi-band large-area surveys to weed out contaminating foreground and background sources.

Of the definite clusters identified so far at  $z > 1$ , five have been found in deep X-ray images (Rosati et al. 1999; Stanford et al. 2002; Rosati et al. 2004; Hashimoto et al. 2004; Mullis et al. 2005). The majority of the others have been identified in pointed observations of radio-source fields (e.g., Hall & Green 1998; Liu et al. 2000; Best et al. 2003; Toft et al. 2003; Wold et al. 2003; Stern et al. 2003). Although it has been well established that extremely red objects (EROs) show strong clustering (e.g., Daddi et al. 2003; Roche, Dunlop, & Almaini 2003; Georgakakis et al. 2005), the only confirmed cluster so far reported at  $z > 1$  from general field surveys is CIG J0848+4453, at  $z = 1.27$  (Stanford et al. 1997). Sawicki et al. (2005) report a strong density enhancement of extremely red objects (EROs), com-

parable to those seen in some radio-source fields, but they have only  $R$  and  $K_S$  imaging and therefore can neither estimate a redshift nor even confirm a common redshift for their objects. A near-miss (as far as redshift is concerned) is the identification from optical/IR imaging (confirmed by spectroscopy) of a rich cluster at  $z = 0.95$  by Barrientos et al. (2004).

We report here the discovery of an apparent cluster of EROs at  $z = 1.34$  from a field optical/IR survey. Since four of the galaxies lie within  $30''$  of a 13th mag star and very close to one another, we have been able to obtain adaptive-optics (AO) imaging to determine their detailed morphologies. We assume a standard concordance cosmological model throughout, with  $H_0 = 70 \text{ km s}^{-1}$ ,  $\Omega_m = 0.3$ , and  $\Omega_\Lambda = 0.7$ .

## 2. OBSERVATIONS, DATA REDUCTION, AND RESULTS

### 2.1. Optical and IR Imaging

The initial discovery of the cluster of red objects came from deep  $R$ ,  $I$ , and  $Z$  imaging obtained as part of the Institute for Astronomy Deep Survey (IfA-DS; we will refer to the cluster as “IDSCL J0749+1018”). The IfA-DS was the result of a proposal from a consortium of astronomers to obtain imaging in 5 fields totalling 2.5 square degrees. The survey data were designed to be used for a wide variety of research projects, including a supernova search (Barris et al. 2004), galactic structure studies, a search for brown dwarfs (Liu et al. 2002), and a search for EROs. The observations were obtained with the SuprimeCam CCD mosaic camera, located at the prime focus of the 8 m Subaru telescope. SuprimeCam comprises ten  $2048 \times 4096$  CCDs and has a  $34' \times 27'$  field of view. Each of the 5 survey fields was covered by two slightly overlapping SuprimeCam fields, giving a final image of approximately  $34' \times 53'$ . The supernova search constrained the design of the survey, requiring observations spaced at a variety of time intervals. Details of the survey, as well as the reduction procedures applied to produce the final images, can be found in Barris et al. (2004).

Because of the vagaries of the weather and of seeing conditions, the final depth in each of the filters varied for the dif-

<sup>1</sup> Based in part on data collected at Subaru Telescope, which is operated by the National Astronomical Observatory of Japan. Some of the data presented herein were obtained at the W.M. Keck Observatory, which is operated as a scientific partnership among the California Institute of Technology, the University of California and the National Aeronautics and Space Administration. The Observatory was made possible by the financial support of the W.M. Keck Foundation.

<sup>2</sup> Alfred P. Sloan Research Fellow

ferent fields. For our ERO searches, we have concentrated on the two fields for which the deepest imaging was obtained, centered at  $04^{\text{h}}38^{\text{m}}40^{\text{s}}$ ,  $-01^{\circ}30'00''$  (“0438 field”) and  $07^{\text{h}}49^{\text{m}}55^{\text{s}}$ ,  $+10^{\circ}09'00''$  (“0749 field”). The limiting magnitudes for  $R$ ,  $I$ , and  $Z$  (Vega system,  $5\sigma$ ,  $1''$ -radius aperture) are, respectively, 26.8, 26.1, and 25.7 for the 0438 field and 26.6, 26.6, and 25.8 for the 0749 field. The general survey of these fields will be discussed elsewhere.

Sources in the 0749 field were identified by running SExtractor (Bertin & Arnouts 1996) on the  $Z$ -band image, using a Gaussian filter matched to the seeing profile. This procedure resulted in a catalog of positions and magnitudes for 145058 sources in the 0.5 square degree field. Colors were found by re-running SExtractor in the two-image mode, in which objects found in the  $Z$ -band image were measured with the same aperture in the registered  $R$  or  $I$ -band image. Catalogs could then be extracted for various magnitude and color cuts.

Because of the limited fields of IR detectors available to us at the time, and because we wished to develop a sample suitable for AO imaging studies of morphology, we focused initially either on fields with high densities of red objects or on red objects close to stars with  $R \leq 14$ . IDSCJ J0749+1018 satisfies both criteria. We observed this and other fields of interest with the CISCO IR camera on the Subaru telescope, obtaining imaging at  $K'$  and  $J$  to distinguish spectral-energy distributions (SEDs) of galaxies comprising old stars from those of heavily reddened starbursts, the other main contributor to the ERO population. The observations were obtained on 2002 Feb 5 UT, with a total of 24 min integration on the cluster field at  $K'$  and 16 min at  $J$ . The seeing FWHM for the  $K'$  image was  $0''.84$ , and that for the  $J$  image was  $1''.1$ . The photometric calibration came from observations of the UKIRT faint standards FS12, FS15, FS122, and FS125 (Hawarden et al. 2001). The cluster field is shown in Fig. 1, and an  $I - K'$  vs.  $K'$  color-magnitude diagram based on magnitudes determined with SExtractor is shown in Fig. 2. Objects in the shaded band are potential candidates for pure old stellar populations with effective ages between 1 Gyr and 3.5 Gyr. We can refine this sample both by bringing to bear photometry in additional bandpasses (which can, e.g., distinguish between the two general types of ERO mentioned above) and by carefully optimizing the photometry. The points shown in red in Fig. 2 are those for which this more extensive and more accurate dataset is consistent with a spectral-energy distribution (SED) due to old stars and for which the final photometry indicates a total  $K'$  mag of  $< 20$  and  $R - K' \gtrsim 6$ .

The SEDs for these 9 galaxies with are shown in Fig. 3. Bruzual & Charlot (2003) solar-metallicity instantaneous-burst models with ages of 3.5 or 2 Gyr are shown for comparison. No great weight should be given to the actual ages implied because of the age-metallicity degeneracy and other issues; however, the generally good fits do indicate that most of these galaxies comprise truly old stellar populations with little reddening or admixture of even a small amount of recent star formation.

It is clear from Fig. 1 that there are additional red objects in the field; many of these have  $R - K' \gtrsim 5$ , which is sometimes taken as a definition for an ERO. Here, however, we will retain the more stringent definition ( $R - K' \geq 6$ , within the photometric errors) in order to define a cleaner sample of old stellar populations.

## 2.2. Spectroscopy

We obtained spectroscopy of the 3 brightest EROs in the cluster field with the Low-Resolution Imaging Spectrograph (LRIS; Oke et al. 1995) on the Keck I telescope on 2003 Jan 30 UT. We used a multi-slit mask with slit widths of  $1''.2$ . The typical seeing PSF during the observations was  $0''.65$ . The 400 line  $\text{mm}^{-1}$ , 8500 Å blazed grating gave a nominal resolution of about 10 Å, and the total integration time was 250 min. The spectrophotometric calibration was obtained from observations of the standards G191B2B and Feige 67. The three galaxies all show spectra characteristic of old stellar populations and have closely similar redshifts near 1.34 (Fig. 4). The redshift fortunately places the strong H and K lines of Ca II in the atmospheric window clear of strong airglow lines between 9000 Å and 9300 Å, leading to quite firm redshifts in spite of occasionally large residuals from strong airglow lines elsewhere in the spectra. These large residuals occur, mainly at the red end of the spectrum, because the fringing pattern in the detector is time variable because of flexure in the instrument, and it cannot entirely be removed.

The photometric and spectroscopic data for the galaxies are summarized in Table 1. While the galaxy designations in the table give sufficiently accurate coordinates to uniquely identify the objects, we often use only the declination portion of the name in figures to avoid crowding.

## 2.3. Adaptive-Optics Imaging

Finally, in order to determine morphologies of some of the galaxies, we carried out AO imaging in the  $K'$  band of a portion of the cluster with the curvature-sensing AO system on the Subaru telescope and the Infrared Camera and Spectrograph (IRCS; Kobayashi et al. 2000) on 2003 Feb 17 UT, using the 22.6 mas  $\text{pixel}^{-1}$  scale. The intrinsic seeing at  $K'$  was  $0''.6$ . The total integration time was 135 min. The AO guide star (USNO B1 1002-0150882) has an  $R$  mag of 13.5, and the galaxies were at distances ranging from  $18''$  to  $28''$  from the guide star. The final image has a FWHM of 91 mas and is shown in Fig. 5.

We used C. Y. Peng’s GALFIT procedure (Peng et al. 2002) to fit the two-dimensional profiles of the galaxies observed with the Subaru AO system. There is a star suitable for determining the PSF conveniently placed in the middle of the group of 4 extremely red galaxies that fit within our AO imaging field, and we find no discernable anisoplanatic distortion across the portion of the field including the galaxies.

## 3. SURFACE-BRIGHTNESS PROFILES AND MORPHOLOGIES

### 3.1. ER 074941.6+101736

This is the brightest of the extremely red galaxies in the AO field and the only one of these four galaxies for which we have a spectroscopic redshift. The two-dimensional model fits are shown on the left side of Fig. 6, and the corresponding radial-surface-brightness profiles are shown on the left side of Fig. 7.

The exponential model is clearly a very poor fit, leaving large residuals at nearly all radii. The de Vaucouleurs model fits quite well overall, nearly as well as the best Sérsic model, but it slightly oversubtracts the center. This behavior is consistent with a break in the profile towards a flatter slope near the center. Examination of the lower part of Fig. 7 (left panel) indicates that one could tweak the de Vaucouleurs profile to obtain an excellent fit to the observations beyond a semi-major axis of  $0''.1$  (840 pc), with a flatter core at smaller radii. The behavior is similar to that of the most luminous ellipticals in the local universe, most of which have “core” profiles

(in the terminology of the Nuker group: Faber et al. 1997; see also Kormendy 1999). With only passive evolution, this galaxy would end up slightly brighter than  $L^*$  at the present epoch. An effective radius  $r_e = 0''.21-0''.25$  corresponds to 1.8–2.1 kpc, compared with a range of 1.7–4.0 kpc and a median of 2.9 kpc for 4 local ellipticals with core profiles and similar luminosities in the sample of Faber et al. (1997).

### 3.2. ER 074940.7+101738

In this case, as is shown on the right sides of Fig. 6 and Fig. 7, it is the de Vaucouleurs model that is clearly unacceptable. As the Sérsic index of  $n = 1.14$  indicates, and as the surface-brightness profiles show, the profile is extremely close to a pure exponential at all radii. This galaxy is likely to be an essentially pure disk, with little or no bulge component. As is evident from the inset for this galaxy in Fig. 5, the galaxy shows no well defined nucleus and weak central concentration.

### 3.3. ER 074941.0+101733

While the panels on the left sides of Fig. 8 and Fig. 9 clearly show that the exponential fit for this galaxy is poor, there is little to choose from between the de Vaucouleurs and the Sérsic profiles, even though the Sérsic profile with index  $n = 6.2$  is formally a slightly better fit. The galaxy appears to be a small elliptical, with an effective radius in the range of 1.0–1.5 kpc and a luminosity about a magnitude fainter than  $L^*$ .

### 3.4. ER 074941.4+101741

For this galaxy, Fig. 8 and Fig. 9 show that the Sérsic model is much superior to either a pure de Vaucouleurs model or a pure exponential model. Nevertheless, the galaxy is highly flattened and clearly has a dominant disk. A composite model, incorporating an  $r^{1/4}$ -law bulge and an exponential disk, fits slightly better than the best Sérsic model and puts 27% of the light in the bulge and 73% in the disk. The consistency of the SED with that of an old stellar population (see Fig. 3) indicates that both the disk and bulge populations in this galaxy are composed of old stars. All of these characteristics suggest a classification as an S0 galaxy much like those we find at the present epoch.

### 3.5. The Kormendy Relation

Our high-resolution imaging of all of these galaxies shows them to be quite regular and symmetric, and their basic morphological parameters appear to be within the range of those of local galaxies today. We can further ask whether the two elliptical galaxies fall close to the mean surface-brightness—effective radius (Kormendy) relation for local ellipticals.

For the bright elliptical galaxy ER 074941.6+101736, we use the de Vaucouleurs  $r_e = 0''.25$  and determine an average  $K'$  surface brightness interior to  $r_e$  of  $\langle \mu \rangle_e = 17.55$  mag arcsec $^{-2}$ . This value must be corrected for the difference in bandpass (observed  $K'$  vs. rest-frame  $V$ ), cosmological surface-brightness dimming, and passive evolution. We assume that the stellar population of the galaxy at the observed redshift can be modelled by a 3.5-Gyr Bruzual & Charlot (2003) solar-metallicity instantaneous burst. Under passive evolution alone, this will correspond to an 12.35-Gyr solar-metallicity model at the present epoch (we use the closest Bruzual & Charlot 2003 model, at 12.25 Gyr). We normalize the redshifted 3.5-Gyr model to give  $K' = 17.55$  through a synthetic  $K'$  filter bandpass and also normalize the rest-frame

12.25-Gyr model by the same factor (the redshifted and rest-frame versions at each age are scaled to give the same bolometric flux). We then correct the 12.25-Gyr model for the  $(1+z)^4$  surface-brightness dimming effect and determine the  $V$  magnitude, again from a synthetic  $V$  filter bandpass, obtaining  $\langle \mu_0 \rangle_e = 18.7$  mag arcsec $^{-2}$ . The uncertainty in this determination from the various assumptions and approximations we have made is at least 0.5 mag.

We compare this value with the determination of the local  $V$ -filter Kormendy relation given by La Barbera et al. (2003), using the same cosmological parameters as we are assuming:

$$\langle \mu_0 \rangle_e = 19.05 + 2.92 \log r_e \quad ,$$

where  $r_e$  is in kpc. The uncertainty in this relation due to the combination of photometric errors and the intrinsic scatter in this relation is  $\sim 0.5$  mag. For ER 074941.6+101736,  $r_e = 2.1$  kpc, giving  $\langle \mu_0 \rangle_e = 20.0$  mag arcsec $^{-2}$ . Thus, this galaxy, although seeming to have slightly higher surface brightness than expected, is not far off the standard Kormendy relation, given the likely uncertainties.

We can carry out this same calculation for the fainter elliptical ER 074941.0+10733. For this galaxy, assuming a 2-Gyr age, we again obtain  $\langle \mu_0 \rangle_e = 18.8 \pm 0.5$  mag arcsec $^{-2}$ . The Kormendy relation for this  $r_e$  gives  $19.2 \pm 0.5$ , so this galaxy falls on the relation within the expected uncertainty.

## 4. SUMMARY AND DISCUSSION

We have been loosely referring to IDSCL J0749+1018 as a cluster, although we admittedly have neither an extensive luminosity function nor X-ray data to back up this designation. Until it is possible to obtain X-ray imaging, we can appeal to a comparison with CIG J0848+4453, at  $z = 1.27$  (Stanford et al. 1997). This grouping of galaxies is confirmed as a cluster by the presence of X-ray emission. This cluster has 6 galaxies with  $K \gtrsim 19.5$  and  $R - K \gtrsim 6$ ; these are galaxies which, through passive evolution alone, would be expected to end up as  $L^*$  galaxies at the present epoch. As it happens, IDSCL J0749+1018 also has 6 such galaxies, so we tentatively identify it as a cluster like CIG J0848+4453, but at a slightly higher redshift. As Fig. 1 shows, there is possible evidence for substructure: 7 of the 9 galaxies with  $R - K \gtrsim 6$  fall into two tight groups of 4 and 3 galaxies, with projected dimensions enclosed within circles of  $15''$  (126 kpc) and  $10''$  (84 kpc), respectively. Whether IDSCL J0749+1018 is truly a virialized cluster or not, it certainly seems to be the case that most of the galaxies are in locally dense environments.

More importantly, we have obtained among the highest-resolution images at restframe  $\sim 0.9 \mu\text{m}$  of a group of galaxies with already old stellar populations when the universe was only a third of its present age. Significantly, even within this small sample of 4 galaxies, we find two galaxies that morphologically appear to be standard ellipticals, one S0, and one that seems to be a pure disk. This variety reinforces the conclusions of Yan, Thompson, & Soifer (2004) that even EROs that are overwhelmingly dominated by old stellar populations show a variety of morphologies. In particular, the presence of an essentially bulgeless disk comprising only old stars re-emphasizes that some disks in the early universe must have formed extraordinarily rapidly and with high rates of star formation (cf. Stockton, Canalizo, & Maihara 2004).

The other main conclusion of this work is that, unlike typical field galaxies at high redshift, and with the exception of the apparent pure disk of old stars, the galaxies for which we have AO imaging look boringly similar to those we see around

TABLE 1  
PROPERTIES OF EXTREMELY RED GALAXIES

Galaxy	$R$	$I$	$Z$	$J$	$K'$	Redshift
ER 074940.7+101738	25.6 +0.2, -0.2	23.81 ±0.05	22.61 ±0.04	21.5 ±0.2	19.46 ±0.07	...
ER 074941.0+101733	26.5 +0.7, -0.4	24.23 ±0.07	23.11 ±0.07	21.5 ±0.2	19.92 ±0.10	...
ER 074941.1+101705	26.4 +0.6, -0.4	23.93 ±0.06	22.69 ±0.04	21.2 ±0.2	19.18 ±0.05	...
ER 074941.4+101711	24.9 +0.1, -0.1	23.07 ±0.03	21.92 ±0.02	20.4 ±0.1	18.53 ±0.03	1.338
ER 074941.4+101741	26.0 +0.4, -0.3	24.39 ±0.09	23.06 ±0.06	21.9 ±0.4	20.04 ±0.11	...
ER 074941.6+101736	24.9 +0.1, -0.1	23.04 ±0.02	21.96 ±0.02	20.4 ±0.1	18.64 ±0.03	1.335
ER 074941.6+101708	25.3 +0.2, -0.2	23.83 ±0.05	22.78 ±0.05	21.4 ±0.2	19.34 ±0.06	...
ER 074941.7+101809	24.8 +0.1, -0.1	23.09 ±0.03	21.93 ±0.02	...	19.00 ±0.04	1.336
ER 074943.1+101707	27.2 +2.6, -0.7	24.28 ±0.08	23.29 ±0.08	22.2 ±0.4	19.84 ±0.09	...

us today. It is quite likely that these galaxies, all within a projected distance of 125 kpc of each other, will suffer some structural changes from mergers and/or harassment (depending on their velocity dispersion). Nevertheless, they are all individually well relaxed, symmetric stellar systems with properties that, through passive evolution alone, would make them indistinguishable from a sample drawn from the present-day galaxy population. This result tends to confirm the common assumption that processes of galaxy formation and evolution are accelerated in denser environments.

This research has been partially supported by NSF grant

AST03-07335. We are grateful to the other investigators in IfA-DS consortium: John Tonry, Ken Chambers, Richard Wainscoat, Nick Kaiser, Pat Henry, Hervé Aussel, Eduardo Martín, and Eugene Magnier; and to Brian Barris, who, with John Tonry, carried out almost all of the actual reduction of the survey images. The authors recognize the very significant cultural role that the summit of Mauna Kea has within the indigenous Hawaiian community and are grateful to have had the opportunity to conduct observations from it.

#### REFERENCES

- Barrientos, L. F., Gladders, M. D., Yee, H. K. C., Infante, L., Ellingson, E., Hall, P. B., & Hertling, G. 2004, *ApJ*, 617, L17
- Barris, B. J., et al. 2004, *ApJ*, 602, 571
- Bertin, E., & Arnouts, S. 1996, *A&AS*, 117, 393
- Best, P. N., Lehnert, M. D., Miley, G. K., & Röttgering, H. J. A. 2003, *MNRAS*, 343, 1
- Bruzual, G. & Charlot, S. 2003, *MNRAS*, 344, 1000
- Daddi, E., Röttgering, H. J. A., Labbé, I., Rudnick, G., Franx, M., Moorwood, A. F. M., Rix, H. W., van der Werf, P. P., & van Dokkum, P. G. 2003, *ApJ*, 588, 50
- Ebeling, H., Edge, A. C., & Henry, J. P. 2001, *ApJ*, 553, 668
- Faber, S. M., et al. 1997, *AJ*, 114, 1771
- Georgakakis, A., Afonso, J., Hopkins, A. M., Sullivan, M., Mobasher, B., & Cram, L. E. 2005, *ApJ*, 620, 584
- Hall, P. B., & Green, R. F. 1998, *ApJ*, 507, 558
- Hashimoto, Y., Barcons, X., Böhringer, H., Fabian, A. C., Hasinger, G., Mainieri, V., & Brunner, H. 2004, *A&A*, 417, 819
- Hawarden, T. G., Leggett, S. K., Letawsky, M. B., Ballantyne, D. R., & Casali, M. M. 2001, *MNRAS*, 325, 563
- Kobayashi, N., et al. 2000, in *Proc. SPIE 4008: Optical and IR Telescope Instrumentation and Detectors*, ed. M. Iye & A. F. Moorwood, p. 1056
- Kormendy, J. 1999, *ASP Conf. Ser.* 182, 124
- La Barbara, F., Busarello, G., Merluzzi, P., Massarotti, M., & Capaccioli, M. 2003, *ApJ*, 595, 127
- Liu, M. C., et al. 2000, *AJ*, 119, 2556
- Liu, M. C., Wainscoat, R., Martín, E. L., Barris, B., & Tonry, J. 2002, *ApJ*, 568, L107
- Mullis, C. R., McNamara, B. R., Quintana, H., Vikhlinin, A., Henry, J. P., Gioia, I. M., Hornstrup, A., Forman, W., & Jones, C. 2003, *ApJ*, 594, 154
- Mullis, C. R., Rosati, P., Böhringer, H., Schwobe, A., Schuecker, P., & Fassbender, R. 2005, *ApJ*, 623, L85
- Oke, J. B., Cohen, J. G., Carr, M., Cromer, J., Dingizian, A., Harris, F. H., Labrecque, S., Lucinio, R., Schaal, W., Epps, H., & Miller, J. 1995, *PASP*, 107, 375
- Peng, C. Y., Ho, L. C., Impey, C. D., & Rix, H.-W. 2002, *AJ*, 124, 266
- Roche, N., Dunlop, J., & Almaini, O. 2003, *MNRAS*, 346, 803
- Rosati, P., Stanford, S. A., Eisenhardt, P. R., Elston, R., Spinrad, H., Stern, D., & Dey, A. 1999, *AJ*, 118, 76
- Rosati, P., et al. 2004, *AJ*, 127, 230
- Sawicki, M., Stevenson, M., Barrientos, L. F., Gladman, B., Mallén-Ornelas, G., & van den Bergh, S. 2005, *ApJ*, in press
- Schlegel, D. J., Finkbeiner, D. P., & Davis, M. 1998, *ApJ*, 500, 525
- Schwobe, A. D., Lamer, G., Burke, D., Elvis, M., Watson, M. G., Schulze, M. P., Szokoly, G., & Urrutia, T. 2004, *Adv. Space Res.*, 34, 2604
- Sérsic, J.-L. 1968, *Atlas de Galaxias Australes*, (Observatorio Astronomico, Cordoba)
- Stanford, S. A., Elston, R., Eisenhardt, P. R., Spinrad, H., Stern, D., & Dey, A. 1997, *AJ*, 114, 2232
- Stanford, S. A., Holden, B., Rosati, P., Eisenhardt, P. R., Stern, D., Squires, G., & Spinrad, H. 2002, *AJ*, 123, 619
- Stern, D., Holden, B., Stanford, S. A., & Spinrad, H. 2003, *AJ*, 125, 2759
- Stockton, A., Canalizo, G., & Maihara, T. 2004, *ApJ*, 605, 37
- Toft, S., Pedersen, K., Ebeling, H., & Hjorth, J. 2003, *MNRAS*, 341, L55
- Wold, M., Armus, L., Neugebauer, G., Jarrett, T. H., & Lehnert, M. D. 2003, *AJ*, 126, 1776
- Yan, L., Thompson, D., & Soifer, B. T. 2004, *AJ*, 127, 1274

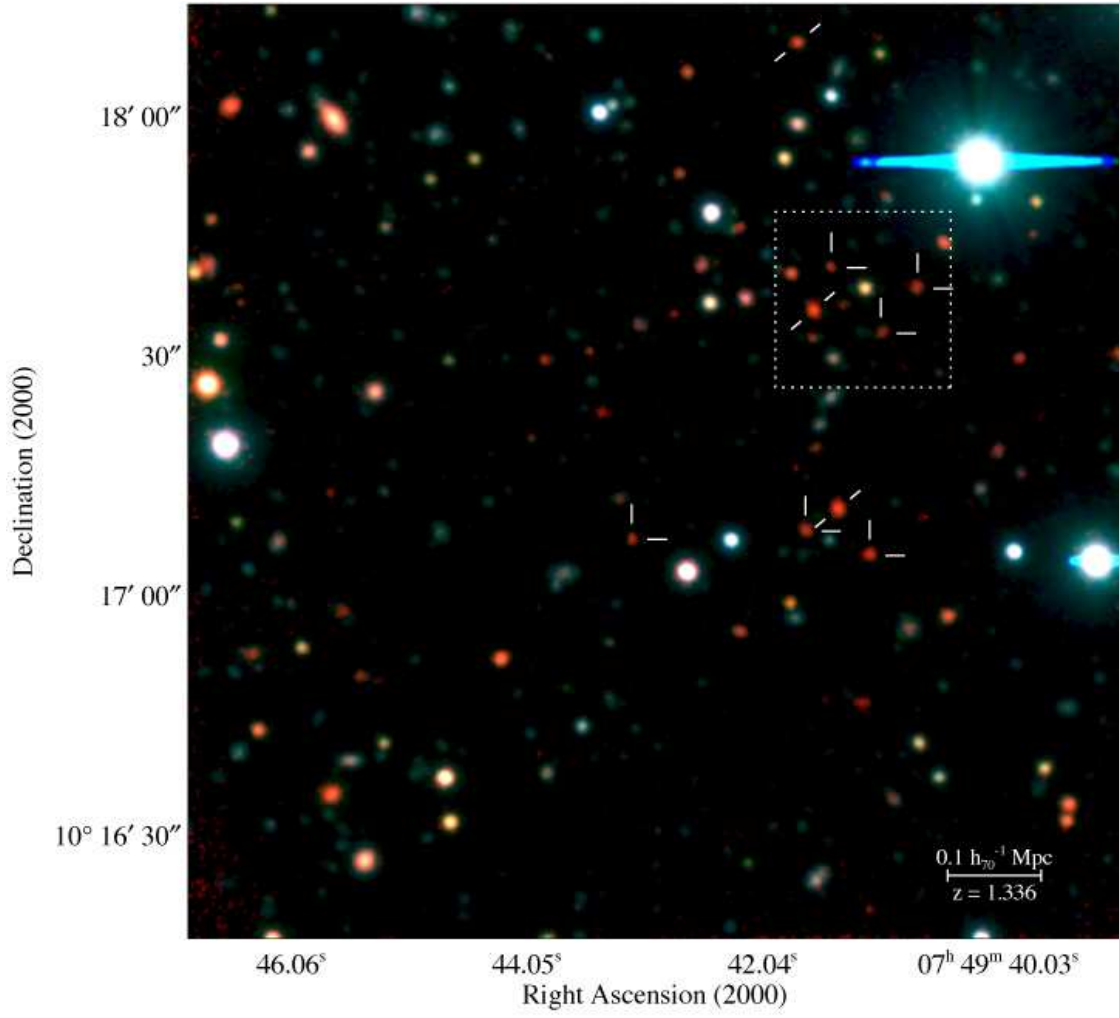


FIG. 1.— The field of the ERO cluster. The color table codes the  $R$  image as blue, the  $I$  image as green, and the  $K'$  image as red. The images have been smoothed to a common PSF. The dotted white square indicates the AO field, and the saturated star to the upper right of the square is the AO guide star. All marked objects have  $R - K' \gtrsim 6$ ; their SEDs shown in Fig. 3. There are clearly other quite red objects in the field. The three objects indicated by diagonal lines have spectroscopic redshifts (see Fig. 4). The angular size of the scale bar is  $11''.9$ .

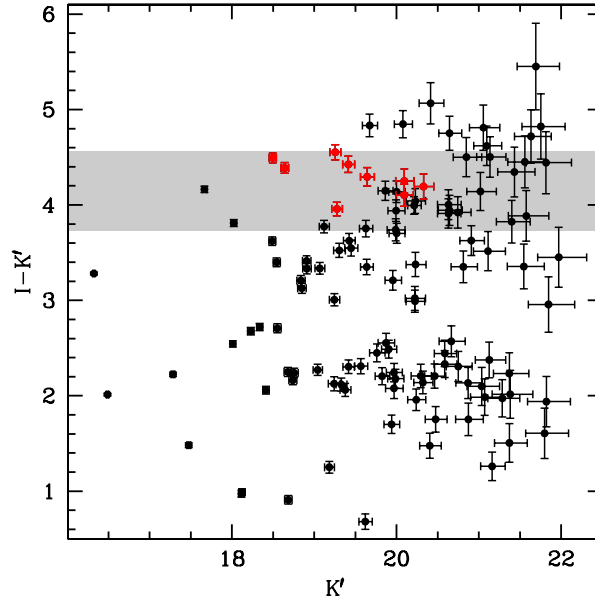


FIG. 2.—  $I - K'$  vs.  $K'$  color-magnitude diagram of objects in the field shown in Fig. 1. The shaded band shows the region populated by “red-sequence” galaxies comprising pure old solar-metallicity stellar populations with ages ranging from 1 Gyr (bottom of band) to 3.5 Gyr (top of band) at a redshift of 1.34. The red points indicate the objects for which the full range of photometry in all available bands gives SEDs consistent with very old stellar populations at  $z \sim 1.34$ . The object in the middle of the band at  $K' = 17.7$  appears to have an old stellar population, but at a somewhat lower redshift. The objects falling above the band at  $K' \sim 20$  tend to have SEDs characteristic of reddened starbursts, as do some of the objects falling in the band.

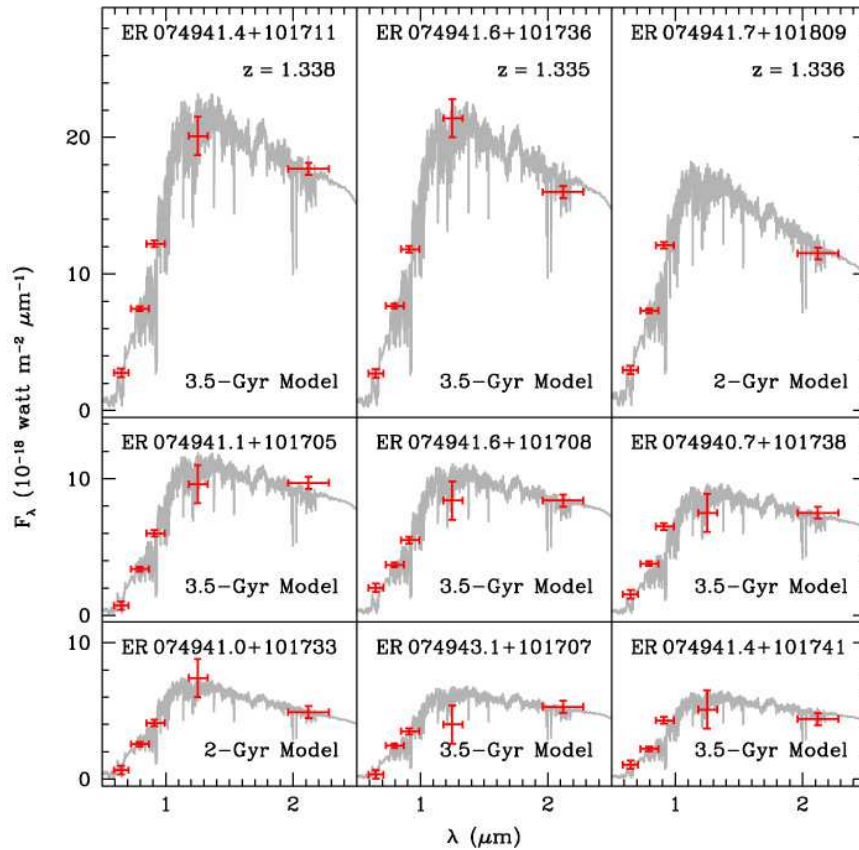


FIG. 3.— Spectral-energy distributions of 9 of the reddest galaxies in the field from optical/IR photometry. The gray traces are reference Bruzual-Charlot (2003) instantaneous-burst models with ages as given in each panel and redshifted to  $z = 1.34$ . Horizontal bars on the photometric points show filter half-transmission widths; vertical bars give  $1-\sigma$  random errors of the photometry. All of these galaxies, with the exception of ER 074943.1+101707 (which may be a dusty starburst), clearly show the strong inflection near rest-frame  $4000 \text{ \AA}$  characteristic of old stellar populations.

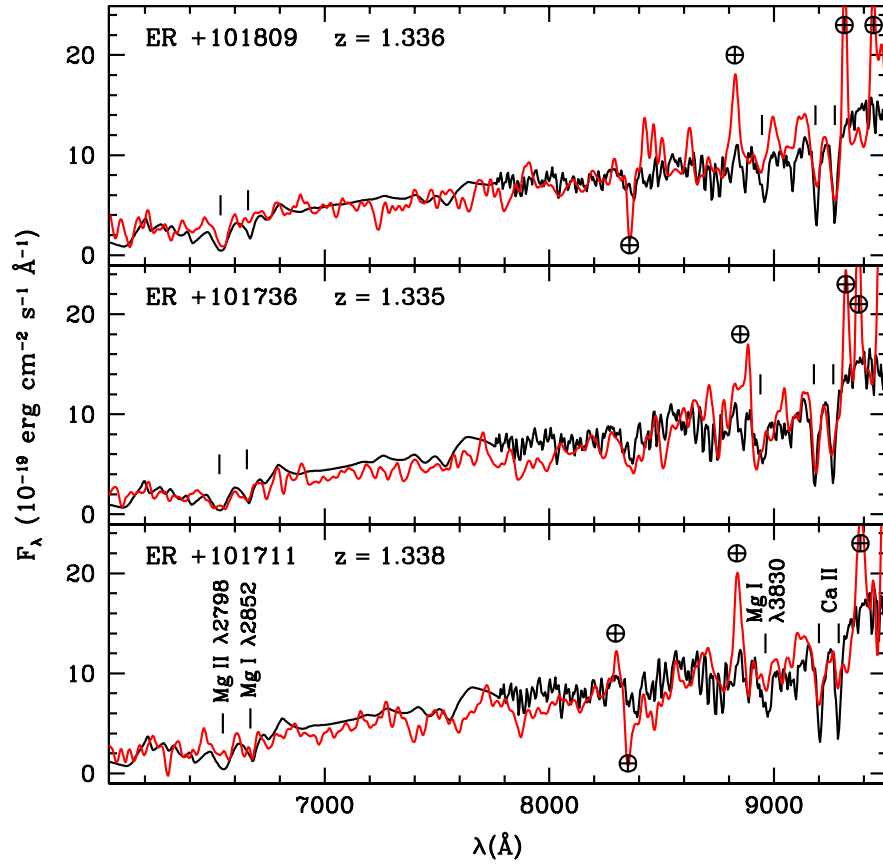


FIG. 4.— Spectra of three galaxies in the cluster field (red lines), overlaid on 3.5 Gyr (bottom two panels) or 2 Gyr (top panel) instantaneous-burst Bruzual & Charlot (2003) models (black lines). Some spectral features in the galaxies are indicated by the vertical lines. The “ $\oplus$ ” symbols indicate positions where strong airglow lines, together with fringing in the CCD, have resulted in significant sky-subtraction residuals. See text for details.

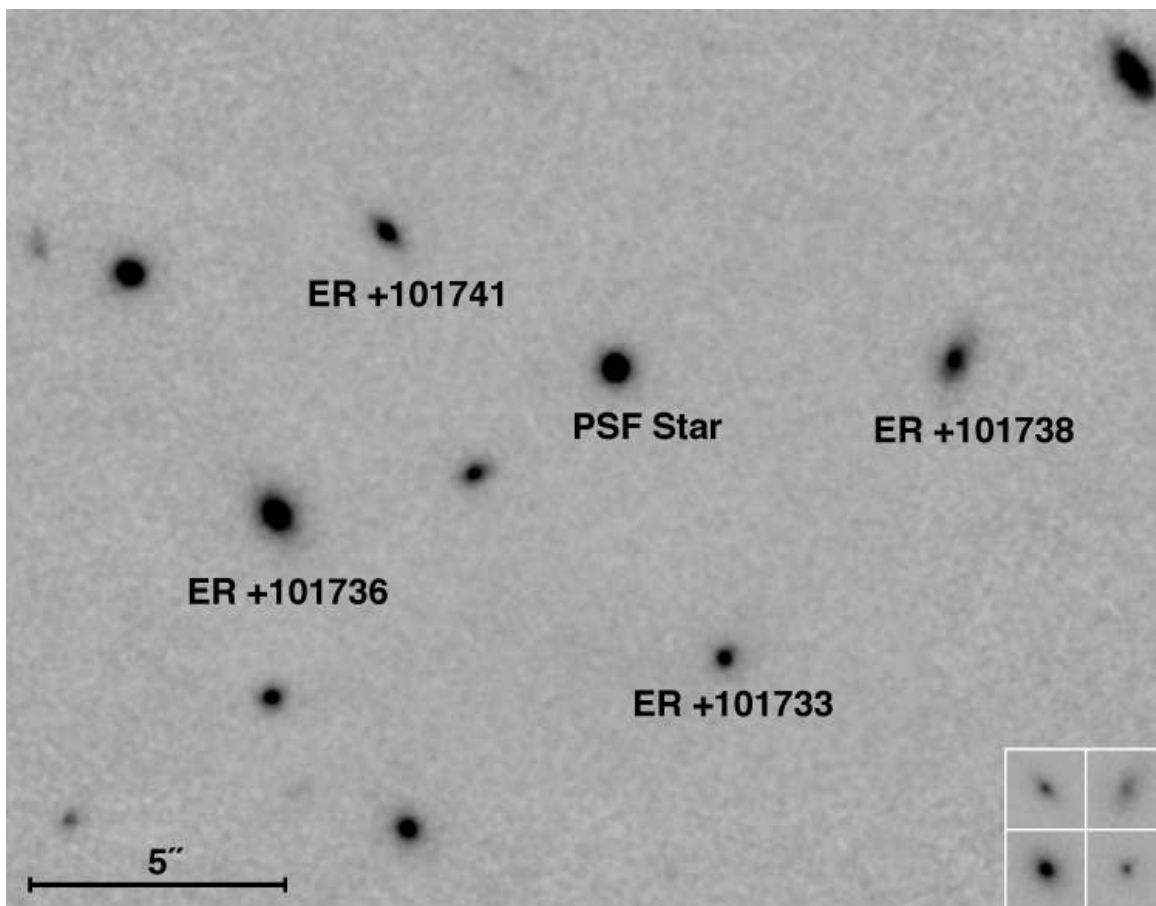


FIG. 5.— The AO image obtained in the  $K'$  band with the Subaru AO system and IRCS. The ERO galaxies are labeled. The insets in the lower-right corner show lower-contrast images in the same rotational order as the main frame. The  $5''$  scalebar corresponds to 42 kpc at  $z = 1.34$ . The main image has been smoothed with a Gaussian with  $\sigma = 2$  pixels; the insets have been similarly smoothed with  $\sigma = 1$  pixel.

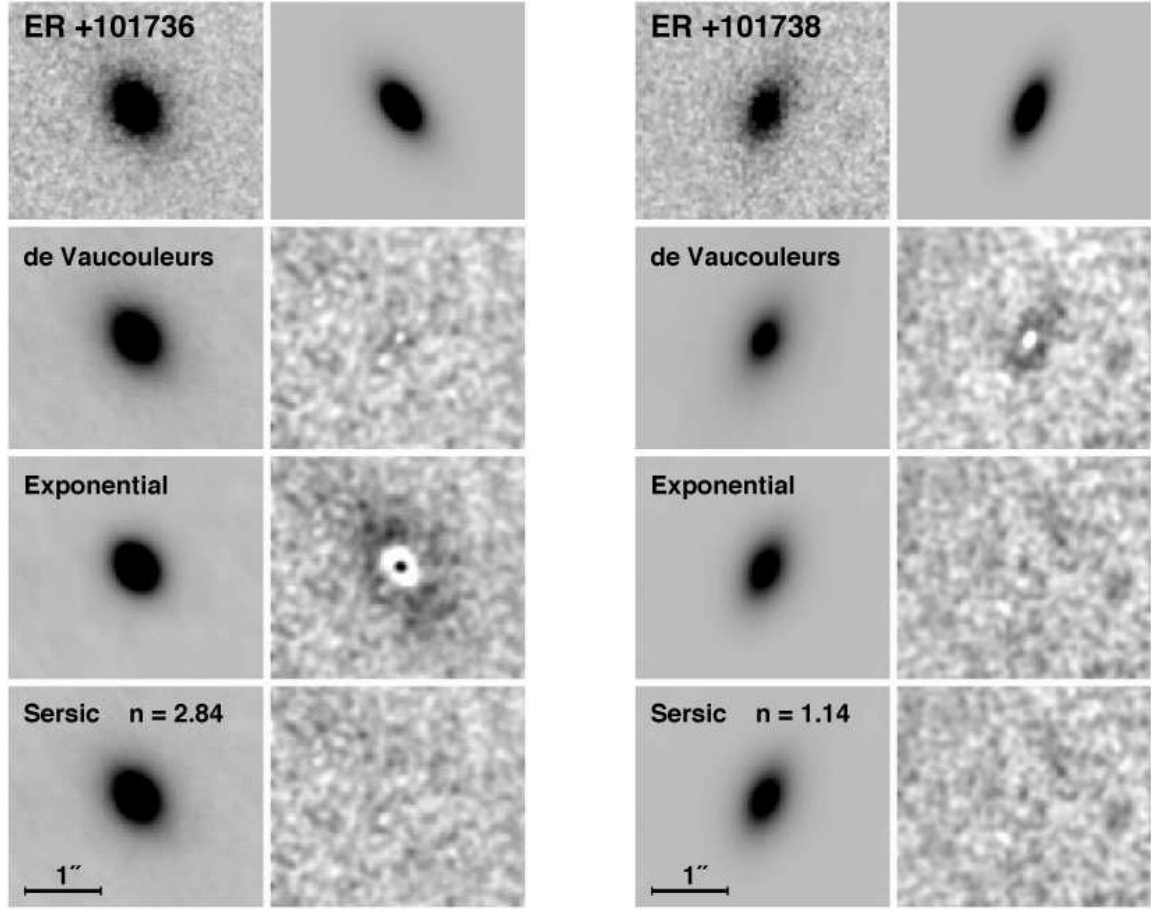


FIG. 6.— Two-dimensional models of ER 074941.6+101736 and ER 074940.7+101738. The upper left panel in each case shows the original AO image; directly below are de Vaucouleurs (“ $r^{1/4}$ -law”), exponential, and Sérsic models, each convolved with the PSF. To the right of each of the models is shown the smoothed residual from the subtraction of the model from the original image. The upper-right panel shows the Sérsic model *without* convolution with the PSF, which gives the best realization of the gross morphology of the galaxy.

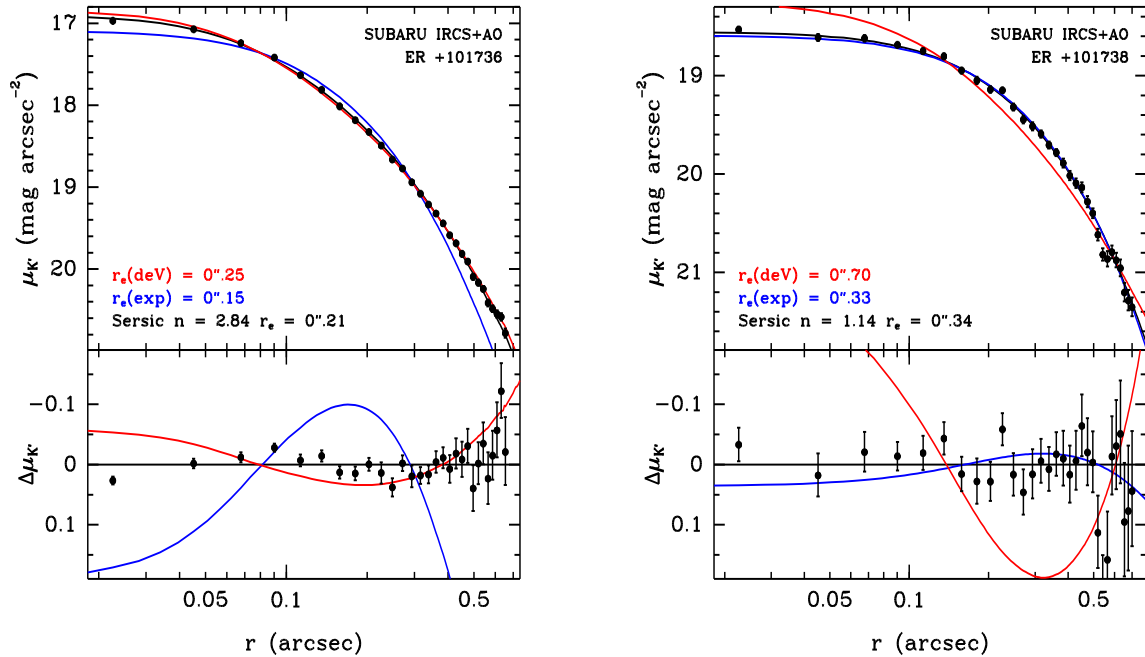


FIG. 7.— PSF-convolved radial-surface-brightness profiles for ER 074941.6+101736 and ER 074940.7+101738. For each galaxy, the top panel shows the model profiles, coded as indicated by color, and with effective radii given for each of the models. The bottom panel shows the deviations of the data points and the other two models from the best Sérsic model.

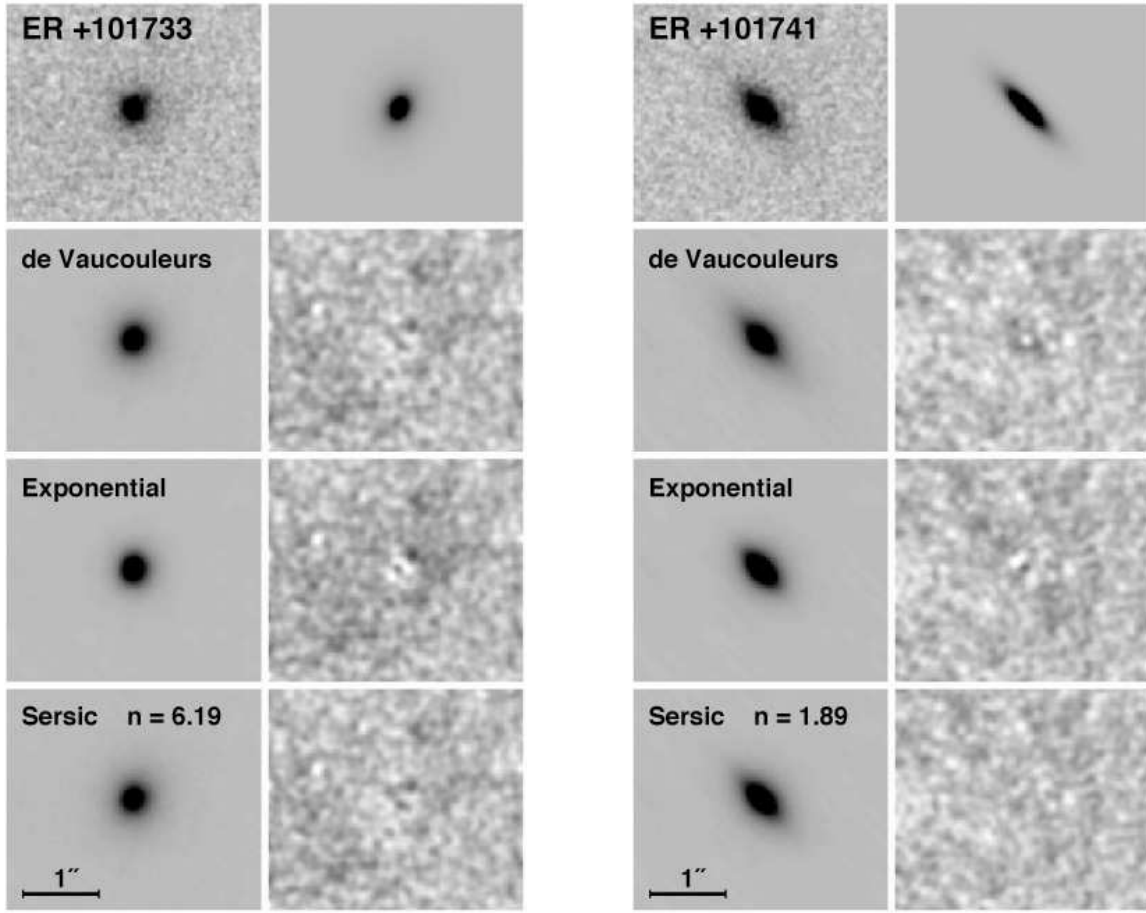


FIG. 8.— Same as Fig. 6, but for ER 074941.0+101733 and ER 074941.4+101741.

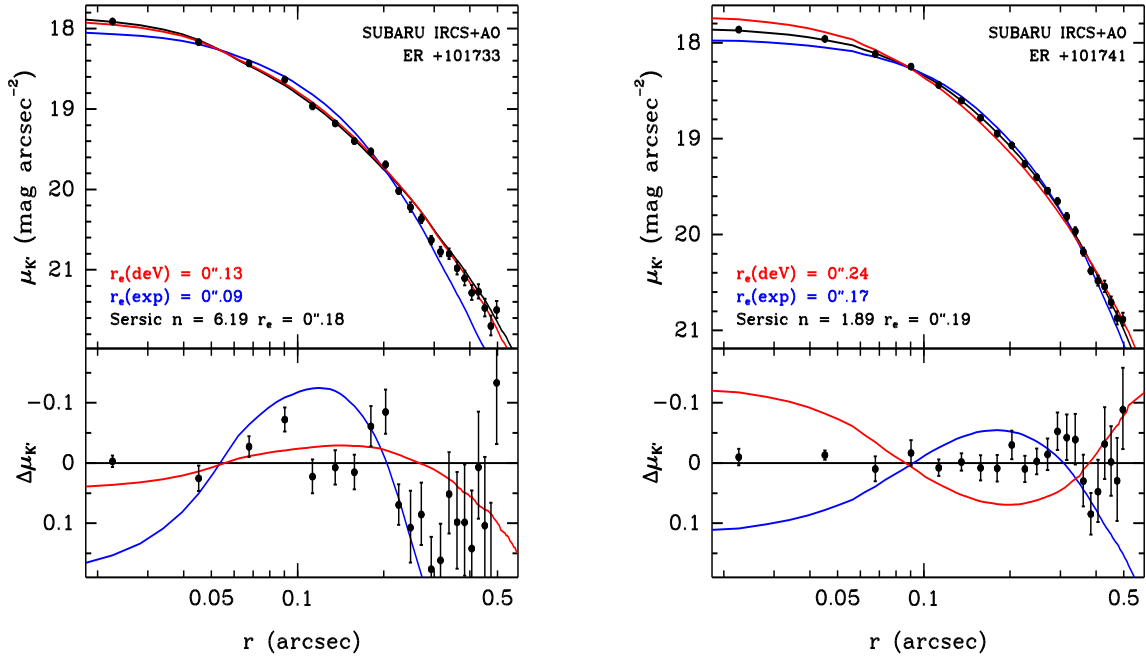


FIG. 9.— Same as Fig. 7, but for ER 074941.0+101733 and ER 074941.4+101741.